Static Structure Factor and Shape of Reptating Telehelic Ionomers in Electric Fields

Song Yan Wu and Gary W. Slater*

Department of Physics, University of Ottawa, Ottawa, Ontario, Canada K1N 6N5

Received August 24, 1992; Revised Manuscript Received December 29, 1992

ABSTRACT: We calculate the exact static structure factor of reptating block copolymers which have a neutral middle block and charged ends. In the presence of an electric field, these telehelic ionomers reptate randomly in their "tubes" but the latter tend to orient along the field axis. If the two ends have different charges, competition between many length scales occurs. The resulting scattering function shows unusual features that are normally characteristic of highly polydisperse mixtures. Our results agree with a recent calculation of the radii of gyration for these molecules. We discuss the possibility of using electric fields to orient long polymers.

1. Introduction

When mixtures of ionomers or polyelectrolytes migrate in neutral gels (or entangled solutions of neutral polymers) under the influence of an applied electric field, the resulting electrophoretic velocity is often molecular-size dependent and can be used to obtain a detailed description of the molecular weight distribution. This technique is widely used in biology to analyze mixtures of nucleic acids[1] or proteins[2] and was recently shown to be applicable to synthetic polyelectrolytes.[3] A simple model of gel electrophoresis, known as the biased reptation model, describes the field-driven migration of large charged polymers as the biased reptation of primitive chains in entanglement tubes that tend to be oriented in the field direction.[4,5] This molecular alignment has indeed been observed by various experimental techniques.[6,7]

Quite generally, the electric field has two effects on these charged molecules. First, it drives them toward the opposite-sign electrode at a velocity that is a function of field intensity, molecular size, gel concentration, and buffer viscosity. Second, because the radius of gyration of the migrating molecules is larger than the entanglement spacing (or pore size), the electric forces and the collisions with the gel fibers deform the molecules substantially.[4-7] The interplay between velocity and molecular shape is often subtle and can be modified by the use of pulsed fields.[4-9] Numerous experimental and theoretical investigations of the relationship between velocity and shape have been published.[4-9]

Recently, the radius of gyration of reptating block copolymers with charged ends and a neutral middle block has been calculated using a new theorem on reptation.[10] These calculations showed that even if the total charge of the molecule is very small, which results in a negligible electrophoretic velocity, substantial molecular orientation can be achieved if the charge is located near the ends of the molecule. However, the radius of gyration does not give a detailed description of the shape of the molecule.

One can define three classes of telehelic block ionomers:[10,11] (a) both ends have charges of the same sign; (b) the two ends have charges of opposite signs; (c) only one end is charged. The static structure factor of class b molecules has been calculated for the special case where the charges were of equal magnitude and the predicted static structure factor was interpreted in terms of the blob picture of chains under stress.[11] However, this is a special case which is probably difficult to realize experimentally.

Ionomers having a charged middle block and end blocks with different (or no) charges form another group of block ionomers. For example, Lumpkin et al.[12] and Slater[13] have studied the case of DNA-like molecules with reduced charges at the ends. Ulanovsky et al.[14] have studied the case of a DNA molecule which has a large neutral globular protein (streptavidin) attached at one of its ends. These molecules have nonzero electrophoretic velocities because of their large electric charges. This leads to an extra term in the equation of motion (our eq 15; see ref 11 for a discussion of this point). The molecules treated in this paper have large uncharged middle blocks and can thus be assumed to have negligible velocities; therefore, the dynamics is due to the Brownian motion of the chains in their reptation tubes.

In this paper, we calculate the exact state structure factor of a general reptating telehelic ionomer. The result can be applied to all three classes mentioned above, regardless of the sign or magnitude of the charges. Our approach uses the biased reptation model. This model has had some success in describing DNA gel electrophoresis, in both constant and pulsed fields. However, it fails when the electric forces are large enough to force the formation of "hernias", molecular loops that penetrate the reptation wall tube (for a good discussion of the model and its limitations, see ref 15). Since the telehelic ionomers considered in this article have uncharged middle blocks and small charged end blocks, such nonreptation modes of migration cannot occur and the biased reptation model is expected to provide an excellent description of the dynamics of these molecules.

The analysis of the resulting structure factor reveals interesting details about the average shape of these copolymers in the presence of an electric field. In particular, we find that the molecules are characterized by many length scales (up to six), including up to two different blob sizes. Competition between the various length scales leads to intriguing features. The radii of gyration agree with those recently calculated using a master equation.[10] Finally, we discuss the possibility of using electric fields to orient large polymers. These suggestions represent an interesting test of the reptation concept.

2. Reptation Model for Telehelic Ionomers

In the reptation model,[16,17] the chain is enclosed in an open-ended tube of contour length L defined by the entanglements surrounding it. The motion of the chain is thus essentially one-dimensional. Tube renewal takes place only from the ends. The Langevin equations for the dynamics of a reptating primitive (or effective) bead–rod

0024-9297/93/2226-1905$04.00/0

chain are given by[17]

$$\mathbf{R}_n(t+\Delta t) = {}^1/_2(1+\eta(t))\mathbf{R}_{n+1}(t) + {}^1/_2(1-\eta(t))\mathbf{R}_{n-1}(t) \quad (1)$$

where $\mathbf{R}_i(t)$ is the position of the ith bead (with $i = 1, 2, \ldots, N+1$), $\eta(t)$ is a stochastic function which takes the value +1 for a forward jump along the tube axis and −1 for a backward jump, and Δt is the average time required by the chain to move over the average distance a between the entanglements (with $a = \langle|\mathbf{R}_{i+1}(t) - \mathbf{R}_i(t)|\rangle$). The boundary conditions for eq 1 are

$$\mathbf{R}_0(t) = \mathbf{R}_1(t) + \mathbf{a}_1(t) \quad (2a)$$

$$\mathbf{R}_{N+2}(t) = \mathbf{R}_{N+1}(t) + \mathbf{a}_N(t) \quad (2b)$$

The first of these equations means that for a backward jump, bead $i = 1$ moves to a new position $\mathbf{R}_0(t)$ while creating a new tube section of orientation $\mathbf{a}_1(t)$. The second equation has a similar meaning for forward jumps.

We assume that forward and backward jumps are equally probable. The relevance of this assumption in the presence of an electric field will be discussed in section 7. Since the end segments of the chain can be charged, the new tube sections $\mathbf{a}_1(t)$ and $\mathbf{a}_N(t)$ cannot be assumed to be randomly oriented, as is normally the case in reptation theories. Instead, $\mathbf{a}_1(t)$ and $\mathbf{a}_N(t)$ will orient preferentially in the field direction.[4] The probability that the charged end segment $\mathbf{a}_{1,N}(t)$ created at time t makes an angle $\theta(t)$ between θ and $\theta + d\theta$ with the field direction is proportional to the Boltzmann factor

$$g_{1,N}(\theta) = \exp(\Theta_{1,N}\cos\theta) \quad (3)$$

where

$$\Theta_{1,N} = \frac{\alpha Q_{1,N} E a}{2k_B T} \quad (4)$$

Here α is a numerical factor which is unity if the end charges $Q_{1,N}$ are uniformly distributed on the end segments. The average projections of the vectors $\mathbf{a}_{1,N}(t)$ on the field axis are thus given by

$$\langle\cos^n\theta\rangle_{1,N} = \frac{\int_0^\pi \sin\theta\, d\theta \cos^n\theta\, g_{1,N}(\theta)}{\int_0^\pi \sin\theta\, d\theta\, g_{1,N}(\theta)} \quad (5)$$

which leads to

$$\langle\cos\theta\rangle_{1,N} = \coth(\Theta_{1,N}) - \frac{1}{\Theta_{1,N}} \quad (6a)$$

$$\approx \frac{\Theta_{1,N}}{3} - \frac{\Theta_{1,N}^3}{45} + \ldots \quad \text{for } \Theta_{1,N} < 1 \quad (6b)$$

$$\langle\cos^2\theta\rangle_{1,N} = 1 + \frac{2}{\Theta_{1,N}^2} - \frac{2\coth(\Theta_{1,N})}{\Theta_{1,N}} \quad (6c)$$

$$\approx \frac{1}{3}\left(1 + \frac{2\Theta_{1,N}^2}{15} + \ldots\right) \quad \text{for } \Theta_{1,N} < 1 \quad (6d)$$

The dimensionless field intensities $\Theta_{1,N}$ and molecular size $N = L/a$ will be used in the rest of this article. Note that the fields can be positive, negative, or zero. In the latter case, one recovers the normal reptation model where the new tube segments are randomly oriented; we then have $\langle\cos\theta\rangle_0 = 0$ and $\langle\cos^2\theta\rangle_0 = {}^1/_3$.

3. The Static Structure Factor

The correlation function $G_{mn}(\mathbf{R},t)$ is defined as the probability that the mth and the nth segments of the chain are separated by a distance $\mathbf{R}$ at time t:

$$G_{mn}(\mathbf{R},t) = \langle\delta\{[\mathbf{R}_m(t) - \mathbf{R}_n(t)] - \mathbf{R}\}\rangle \quad (7)$$

The structure factor $S(\mathbf{q},t)$ measured in elastic neutron scattering is defined in terms of the Fourier transform of $G_{mn}(\mathbf{R},t)$:

$$S(\mathbf{q},t) = \frac{1}{N^2}\sum_{mn} F_{mn}(\mathbf{q},t) \quad (8)$$

where

$$F_{mn}(\mathbf{q},t) = \int d^3R \exp(i\mathbf{q}\cdot\mathbf{R})\, G_{mn}(\mathbf{R},t) = \langle\exp\{i\mathbf{q}\cdot[\mathbf{R}_m(t) - \mathbf{R}_n(t)]\}\rangle \quad (9)$$

The averages $\langle\ldots\rangle$ are carried out for an ensemble of identical chains. Note that since the reptation model does not contain short length scale details, our description is limited to $qa < 1$.

From eqs 1 and 9, the Fourier component $F_{mn}(\mathbf{q},t)$ satisfies the equation of motion

$$F_{mn}(\mathbf{q},t+\Delta t) = {}^1/_2 F_{m+1,n+1}(\mathbf{q},t) + {}^1/_2 F_{m-1,n-1}(\mathbf{q},t) \quad (10)$$

With $l = ma$, $l' = na$, and $F(l,l',\mathbf{q},t) \equiv F_{mn}(\mathbf{q},t)$, the continuum limit of eq 10 for large N gives the following differential equation:

$$\frac{\partial F(l,l',\mathbf{q},t)}{\partial t} = D_c\left(\frac{\partial}{\partial l} + \frac{\partial}{\partial l'}\right)^2 F(l,l',\mathbf{q},t) \quad (11)$$

The corresponding boundary conditions obtained from eqs 2a, 2b, and 9 are[11]

$$\frac{\partial F(l,l',\mathbf{q},t)}{\partial l'} = \left(\frac{iz_1 + x_1}{L}\right)F(l,l',\mathbf{q},t) \quad \text{at } l' = 0 \quad (12a)$$

$$\frac{\partial F(l,l',\mathbf{q},t)}{\partial l} = \left(\frac{-iz_1 + x_1}{L}\right)F(l,l',\mathbf{q},t) \quad \text{at } l = 0 \quad (12b)$$

$$\frac{\partial F(l,l',\mathbf{q},t)}{\partial l} = \left(\frac{iz_N - x_N}{L}\right)F(l,l',\mathbf{q},t) \quad \text{at } l = L \quad (12c)$$

$$\frac{\partial F(l,l',\mathbf{q},t)}{\partial l'} = \left(\frac{-iz_N - x_N}{L}\right)F(l,l',\mathbf{q},t) \quad \text{at } l' = L \quad (12d)$$

where, with ψ the angle between $\mathbf{q}$ and $\mathbf{E}$,

$$x_i = \frac{L}{2a}\langle[\mathbf{q}\cdot\mathbf{a}_i(t)]^2\rangle = \frac{1}{2}q^2 La\left[\frac{1}{2}\sin^2(\psi) + \left(\cos^2(\psi) - \frac{1}{2}\sin^2(\psi)\right)\langle\cos^2\theta\rangle_i\right] \quad (13a)$$

$$z_i = \frac{L\langle\mathbf{q}\cdot\mathbf{a}_i(t)\rangle}{a} = Lq\cos(\psi)\langle\cos\theta\rangle_i \quad (13b)$$

To solve eqs 11 and 12, we use the variables[11]

$$s = \frac{l + l'}{L}; \quad p = \frac{l - l'}{L} \quad (14)$$

Equations 11 and 12 then become

$$\frac{\partial F(s,p,\mathbf{q},t)}{\partial t} = \frac{4D_c}{L^2}\frac{\partial^2 F(s,p,\mathbf{q},t)}{\partial s^2} \quad (15)$$

$$\left(\frac{\partial}{\partial s} - \frac{\partial}{\partial p}\right)F(s,p,\mathbf{q},t) = (iz_1 + x_1)F(s,p,\mathbf{q},t) \quad \text{at } s = p \quad (16a)$$

$$\left(\frac{\partial}{\partial s} + \frac{\partial}{\partial p}\right)F(s,p,\mathbf{q},t) = (-iz_1 + x_1)F(s,p,\mathbf{q},t) \quad \text{at } s = -p \quad (16b)$$

$$\left(\frac{\partial}{\partial s} + \frac{\partial}{\partial p}\right)F(s,p,\mathbf{q},t) = (iz_N - x_N)F(s,p,\mathbf{q},t) \quad \text{at } s = 2 - p \quad (16c)$$

$$\left(\frac{\partial}{\partial s} - \frac{\partial}{\partial p}\right)F(s,p,\mathbf{q},t) = (-iz_N - x_N)F(s,p,\mathbf{q},t) \qquad \text{at } s = 2 + p \tag{16d}$$

The boundary conditions (16a) and (16c) are for $p > 0$, while (16b) and (16d) are for $p < 0$. Finally, the static structure factor $S(\mathbf{q},t)$, in terms of the relative variables s and p, is given by

$$S(\mathbf{q},t) = \frac{1}{2}\int_0^1 ds \int_{-s}^{s} dp\, F(s,p,\mathbf{q},t) + \frac{1}{2}\int_1^2 ds \int_{s-2}^{2-s} dp\, F(s,p,\mathbf{q},t) \tag{17}$$

In the steady state, i.e., for $t \to \infty$, we have $\partial F/\partial t = 0$, and the solution of eq 15 is

$$F_\infty(s,p,\mathbf{q}) = A(p)s + C(p) \tag{18}$$

where the "constants" of integration $A(p)$ and $C(p)$ are to be found from the conditions (16). We will not study the time dependence of $S(\mathbf{q},t)$ in this article.

4. Zero-Field Case

As a useful example, we derive here the static structure factor for the equilibrium (zero-field) case. According to eqs 6 and 13, we have, for $\mathbf{E} = 0$,

$$z_1 = z_N = 0 \tag{19a}$$

$$x_1 = x_N \equiv x^{(0)} = q^2\frac{La}{6} = q^2R_g^{\,2} \tag{19b}$$

where $R_g = (La/6)^{1/2}$ is the radius of gyration of the chain in equilibrium. The solution of eqs 15 and 16 is then

$$F_{equ}(s,p,\mathbf{q}) = \exp(-q^2R_g^{\,2}|p|) \tag{20}$$

from which eq 17 gives

$$S_{equ} = D(q^2R_g^{\,2}) \tag{21a}$$

$$\approx 1 - {}^1/_3 q^2R_g^{\,2} + \ldots \qquad \text{for } qR_g \ll 1 \tag{21b}$$

$$\approx \frac{2}{q^2R_g^{\,2}} + \ldots \qquad \text{for } qR_g \gg 1 \tag{21c}$$

where $D(x) = 2(x - 1 + e^{-x})/x^2$ is the Debye function. These well-known results indicate that $S_{equ}(\mathbf{q})$ measures the average dimensions of the equilibrium chain.

5. Static Structure Factor in the General Case

We now derive the static structure factor for the general case. With the scattering factors $z_{1,N}$ and $x_{1,N}$, we can solve eqs 16a and 16c for $A(p)$ and $C(p)$, as defined by eq 18, to obtain

$$A(p) = K_1 e^{-(x_1+iz_1)p} + K_2 e^{-(x_N-iz_N)p} \tag{22}$$

$$C(p) = \frac{1}{iz_1 + iz_N + x_1 - x_N}[K_1 e^{-(x_1+iz_1)p}(x_1p - x_Np - 2x_1 + 2x_N + 2 + iz_1p + iz_Np - 2iz_1 - 2iz_N) + K_2 e^{-(x_N-iz_N)p}(x_Np - iz_Np + 2 - iz_1p - x_1p)] \tag{23}$$

where the constants $K_{1,2}$ are fixed by the conditions

$$\lim_{p\to 0} F_\infty(s,p,\mathbf{q}) = 1 \tag{24a}$$

$$\lim_{z_1\to 0}\lim_{z_N\to 0}\lim_{x_1\to x^{(0)}}\lim_{x_N\to x^{(0)}} F_\infty(s,p,\mathbf{q}) = F_{equ}(s,p,\mathbf{q}) \tag{24b}$$

We find $K_1 = -K_2 = -{}^1/_2$, from which eqs 18, 22, and 23 give

$$F_\infty(s,p>0,\mathbf{q}) = {}^1/_2[e^{-(x_N-iz_N)p} - e^{-(x_1+iz_1)p}]s + \frac{1}{2(iz_1 + iz_N + x_1 - x_N)}[e^{-(x_N-iz_N)p}(-x_1p + x_Np + 2 - iz_1p - iz_Np) - e^{-(x_1+iz_1)p}(x_1p - x_Np - 2x_1 + 2x_N + 2 + iz_1p + iz_Np - 2iz_1 - 2iz_N) \tag{25}$$

Similarly, solving eqs 16b, 16d, 24a, and 24b for $p < 0$, we get

$$F_\infty(s,p<0,\mathbf{q}) = {}^1/_2[e^{(x_N+iz_N)p} - e^{-(x_1-iz_1)p}]s + \frac{1}{2(-iz_1 - iz_N + x_1 - x_N)}[e^{(x_N+iz_N)p}(x_1p - x_Np + 2 - iz_1p - iz_Np) - e^{(x_1-iz_1)p}(-x_1p + x_Np - 2x_1 + 2x_N + 2 + iz_1p + iz_Np + 2iz_1 + 2iz_N) \tag{26}$$

With eqs 25 and 26, eq 17 gives

$$S_\infty(\mathbf{q}) = \Omega(x_1,z_1) + \Omega(x_N,z_N) + \phi(z_1,x_1,z_N,x_N) + \phi(z_N,x_N,z_1,x_1) \tag{27}$$

Here, $\Omega(x,z)$ and $\phi(z_i,x_i,z_j,x_j)$ are defined as

$$\Omega(x,z) = \frac{x^5 - 2x^4 + 2x^3 + 2x^3z^2 + xz^4 - 6xz^2 + 2z^4}{(x^2+z^2)^3} - \frac{2e^{-x}[(x^3 - 3xz^2)\cos(z) + (z^3 - 3x^2z)\sin(z)]}{(x^2+z^2)^3} \tag{28}$$

$$\phi(z_i,x_i,z_j,x_j) = \{2(z_i^4 - x_i^4 + x_i^3x_j + z_i^3z_j + z_i^2x_ix_j + x_i^2z_iz_j + x_i^3 - x_i^2x_j + x_jz_i^2 - 2x_iz_iz_j)\}/\{[(x_i - x_j)^2 + (z_i + z_j)^2](x_i^2 + z_i^2)^2\} + \{2e^{-x_i}[(x_i^2x_j - x_i^3 - z_i^2x_j + 3x_iz_i^2 + 2x_iz_iz_j)\cos(z_i) + (x_i^2z_j - z_i^2z_j - z_i^3 + 3x_i^2z_i - 2x_iz_iz_j) \times \sin(z_i)]\}/\{[(x_i - x_j)^2 + (z_i + z_j)^2](x_i^2 + z_i^2)^2\} \tag{29}$$

In the next sections we study the various features predicted to occur on the $S_\infty(\mathbf{q})$ vs q curves using our general solution given by eqs 27–29. Note that eq 27 reduces to eq 48 of ref 11 when $Q_1 = -Q_N$, as it should be.

6. Results

The steady-state static structure factor $S_\infty(\mathbf{q})$ depends entirely on the parameters $x_{1,N}$ and $z_{1,N}$ which come from the four boundary conditions given by eqs 16. As mentioned before, there are four classes of telehelic ionomers, defined according to their boundary conditions $x_{1,N}$ and $z_{1,N}$, i.e., according to their end-segment charges Q_1 and Q_N. Figure 1 shows schematic examples for each of the four classes. In class a, we have $Q_1Q_N < 0$, and the end segments point in opposite directions in an electric field, thus giving the chain an elongated I-shaped conformation. In class b, $Q_1Q_N > 0$, and the end segments are pointing in the same direction, giving a typical J-shaped conformation. In class c, one charge is zero while the other is finite; the electric field then affects only the part of the chain for which the reptation tube has been generated by the charged end segment, the rest of the chain staying in a random-walk conformation. Finally, when $Q_1 = Q_N = 0$, the electric field does not modify the evolution of the tube (class d is thus same as the zero-field case treated in section 4).

Before we discuss the static structure factor for the three nontrivial classes a–c, we introduce below the length scales involved in the problem, a useful theorem on reptation, and finally the value of the radius of gyration in some special cases.

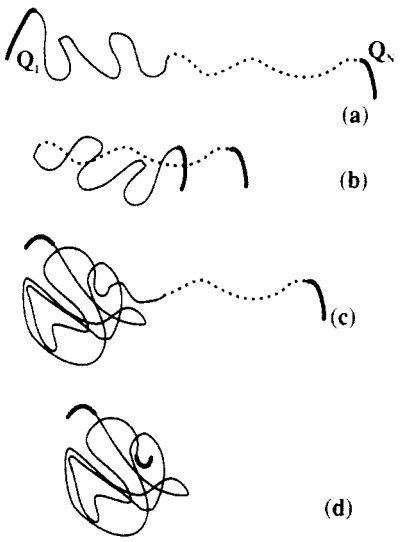

Figure 1. Schematic high-field conformations for the four classes of charged polymer chains. (a) $Q_1Q_N < 0$: the end segments point in opposite directions with two anisotropic orientation lengths $\xi_1^{\parallel}$ and $\xi_N^{\parallel}$, and the chain orients to take an I-shape. (b) $Q_1Q_N > 0$: the end segments point in the same direction with two anisotropic orientation lengths $\xi_1^{\parallel}$ and $\xi_N^{\parallel}$, giving a J-shaped conformation. (c) Only one end segment is charged: this segment orients a part of the chain with an anisotropic orientation length $\xi_N^{\parallel}$, while the rest stays in a (zero-field-like) random-walk conformation. (d) $Q_1 = Q_N = 0$: the chain has a random-walk conformation. Dashed and solid lines show different degrees of orientation; the end segments are thicker. These conformations represent average molecular shapes and orientations, not snapshots.

6.1. The Length Scales. There are six important length scales in the problem. The first one is a, the average distance between entanglements. Usually, we take a as a constant fixed by the topology of the problem; in a gel matrix, a would be given by the average pore size. The second one is the wavelength $1/q$ used to probe the structure; the reptation theory is valid only for $qa < 1$. A third length is the length of the tube $L = Na$, which is proportional to the length of the molecule itself.

The fourth and the fifth length scales are related to the boundary condition parameters $x_{1,N}$ and $z_{1,N}$. The equilibrium conformation ($Q\mathbf{E} = 0$) is characterized by the radius of gyration R_g; to first order in E, the ratio between the lengths R_g and q^{-1} defines the parameters x_i. The electric force $Q_i\mathbf{E}$ brings in the anisotropic conformation length ξ_i^{ψ} defined as

$$\xi_i^{\psi} = L|\langle \cos\theta \rangle_i \cos(\psi)| \tag{30}$$

This length measures the orientation (at an angle ψ from $\mathbf{E}$) of a tube generated by an end segment having an average projection $\langle \cos\theta \rangle$ on the field direction. The ratio between ξ_i^{ψ} and q^{-1} defines the parameter z_i. Of course, $\xi_i^{\perp} = 0$ since the field does not induce order in the transverse plane. Note that if $|Q_1| \neq |Q_N|$, eq 30 defines two lengths ξ_i^{ψ} when both ends of the molecule are charged.

The boundary conditions show a competition between R_g and ξ_i^{ψ} (if at least one end segment is charged) since $z_i^2/x_i \approx (\xi_i^{\psi}/R_g)^2$. At low fields, $R_g > \xi_i^{\psi}$, and x_i leads to almost isotropic random-walk conformations (the dependence of x_i on $\langle \cos^2\theta \rangle_i$ makes it slightly anisotropic). At large fields, however, we have $R_g < \xi_i^{\psi}$ and $R_g > \xi_i^{\perp}$, and the chain conformations are oriented in the field direction (over a length $\sim\xi_i^{\parallel}$), but slightly shrunk in the transverse plane.

For class a chains, strong electric forces lead to an I-shaped conformation (Figure 1a), with an average end-to-end distance of order $\xi^{\parallel}$. For class b, the chains fold in two (Figure 1b), with both ends pointing in the field direction; the length of the two arms of the J-shaped conformation are then proportional to the lengths $\xi_i^{\parallel}$ (at high fields). In class c, a part of the chain is oriented in the field direction, with an isotropic characteristic length scale $\xi_N^{\parallel}$, while the rest stays in a quasi-isotropic random-walk conformation with a length scale R_g (see Figure 1c).

The last length scale is the blob size b_i defined by $b_i = R_g^2/\xi_i^{\psi}$. It can be interpreted in the following way: We will see in section 6.4 that for $q > 1/b_i$, the static structure factor is the same as for an equilibrium chain. This means that the electric forces are not strong enough to modify the random-walk conformation over lengths smaller than b_i. A volume of size b_i^3 contains $n_i = b_i^2/a^2$ segments if these segments stay in a random-walk conformation. We can describe the three kinds of (average) oriented conformations (Figure 1) as series of N/n_i random-walk "blobs" of size b_i aligned by the electric forces (which act effectively over lengths larger than b_i). The dimension of an oriented conformation is therefore proportional to $(N/n_i)b_i = \xi_i^{\psi}$, as expected. Since the field does not align the blobs in the transverse direction, they act as an effective segment of length b_i following a transverse random walk with dimension $(N/n_i)^{1/2}b_i \approx R_g$. Of course, if the charges Q_1 and Q_N are of unequal magnitudes, two different blob sizes b_i and length scales ξ_i^{ψ} will compete. This leads to interesting effects, as we will see later.

6.2. A Useful Theorem on Reptation. We now briefly review a recent theorem on reptation that will be most useful to interpret our results.[10] In the reptation model, the chain can be represented by a series of N vector segments $\mathbf{r}_i$ with $\mathbf{r}_i = \mathbf{R}_{i+1} - \mathbf{R}_i$ ($1 \le i \le N$), where $\mathbf{r}_1$ and $\mathbf{r}_N$ are thus the end segments of the chain. Since new tube sections are created only when the $\mathbf{r}_1$ and $\mathbf{r}_N$ end segments leave the original tube, all orientations $\mathbf{r}_i$ of the N tube segments have been chosen in the past by one of the two end segments (we neglect here tube leakage or any other degree of freedom not included in the ideal reptation model). Because the chain is continuous, the n_+ segments that owe their present orientation to past $\mathbf{r}_N \rightarrow \mathbf{a}_N$ jumps are consecutive, starting from the end segment $\mathbf{r}_N$. Similarly, the $n_- = N - n_+$ segments oriented in the past by $\mathbf{r}_1 \rightarrow \mathbf{a}_1$ jumps are consecutive, starting from $\mathbf{r}_1$. If we denote by $g(n_+,t)$ the probability that n_+ segments of the chain owe their orientation at time t to past $\mathbf{r}_N \rightarrow \mathbf{a}_N$ jumps, we have, in the steady state[10] (i.e., when $\partial g(n_+)/\partial t = 0$)

$$g(n_+,t) \equiv g(n_+) = \frac{1}{(N+1)^{-1}} \quad \text{with } 0 \le n_+ \le N \tag{31}$$

We get a surprising result: In the steady state, all tube segments (including $\mathbf{r}_1$ and $\mathbf{r}_N$) have an equal probability of having been oriented by either end of the tube. This result has profound consequences. For instance, the relative weights of the two competing length scales ξ_1^{ψ} and ξ_N^{ψ} will be randomly distributed and not peaked around $^1/_2$, as one might naively expect. This will be the basis for our understanding of the static structure factor of telehelic ionomers.

6.3. Radii of Gyration. The radius of gyration is the average distance squared between the different parts of the object and its center of mass. It describes the distribution of matter around the center of mass and therefore gives information on the average size and shape

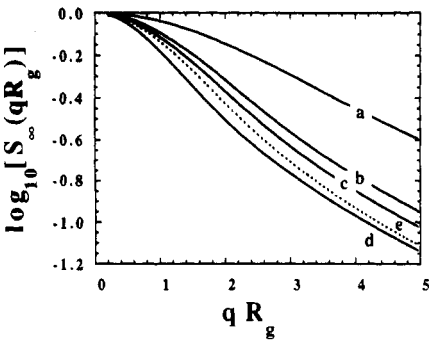

Figure 2. Long-wavelength behavior of the steady-state structure factor $S_\infty^\perp$ (curves a–c), S_{equ} (curve e), and $S_\infty^\parallel$ (curve d): log (S) vs qR_g is plotted for $N = 1000$ and different charged ends. (a) $\Theta_1 = 10$, $\Theta_N = 10$; (b) $\Theta_1 = 3$, $\Theta_N = -3$; (c) $\Theta_1 = 3$, $\Theta_N = 0$; (d) $\Theta_1 = 0.05$, $\Theta_N = -0.05$; (e) $\Theta_1 = 0$, $\Theta_N = 0$. For small orientations, the chain is almost unperturbed by the field.

that the end-to-end distance does not provide. It can be measured by various scattering techniques in the case of polymers. The radius of gyration for the three classes of charged chains has been shown to be given by[10]

$$R_{g\perp}^2 = \frac{Na^2}{12}\langle \sin^2\theta\rangle \tag{32a}$$

$$R_{g\parallel}^2 = \frac{Na^2}{6}\langle \cos^2\theta\rangle + \frac{N^2a^2}{12}\langle \cos\theta\rangle^2 \quad \text{for } Q_1 = -Q_N \tag{32b}$$

$$R_{g\parallel}^2 = \frac{Na^2}{6}\langle \cos^2\theta\rangle + \frac{N^2a^2}{20}\langle \cos\theta\rangle^2 \quad \text{for } Q_1 = Q_N \tag{32c}$$

$$R_{g\parallel}^2 = \frac{Na^2}{6} + \frac{Na^2}{12}\langle \cos^2\theta\rangle + \frac{N^2a^2}{30}\langle \cos\theta\rangle^2 \quad \text{for } Q_1 = 0;\ Q_N \neq 0 \tag{32d}$$

We will compare our results with these equations below. Note however that eqs 32b and 32c apply only if the charges are of equal magnitude.

6.4. Structure Factor for Small Orientation. At low field intensity and/or for $\psi \cong \pi/2$, we have $\xi_i^\psi \ll R_g$ and the chain is almost unperturbed by the field. From eq 27, we then obtain

$$S_\infty^\psi(\mathbf{q}) \approx 1 - \frac{x_1^\psi}{6} - \frac{x_N^\psi}{6} + \ldots \approx 1 - \frac{x^\psi}{3} + \ldots \quad \text{for } (q\xi_1^\psi;\ q\xi_N^\psi) \ll qR_g < 1 \tag{33a}$$

$$\approx \frac{1}{x_1^\psi} + \frac{1}{x_N^\psi} + \ldots \approx \frac{2}{x^\psi} + \ldots \quad \text{for } (q\xi_1^\psi;\ q\xi_N^\psi) \ll qR_g \text{ and } qR_g > 1 \tag{33b}$$

where we used $x_1^\psi \approx x_N^\psi \equiv x^\psi \approx x^{(0)} = q^2R_g^2$. We find that the structure factor is almost unchanged compared to eq 21, as shown on Figure 2 for some selected cases. In other words, the radius of gyration is basically unchanged in these limits.

6.5. Parallel Structure Factor for High Field Intensities. At fields large enough to have $\xi^\parallel \gg R_g$ for at least one end segment (1 or N), we have to distinguish between four different wavelength regimes.

6.5.1. Parallel Structure Factor for $1 > q\xi^\parallel \gg qR_g$. From eq 27, the static structure factor in this regime can then be written as

$$S_\infty^\parallel(\mathbf{q}) \approx 1 - \frac{(z_1^\parallel)^2 + (z_N^\parallel)^2}{30} + \frac{z_1^\parallel z_N^\parallel}{60} - \frac{x_1^\parallel}{6} - \frac{x_N^\parallel}{6} + \ldots \tag{34}$$

Since the last two terms are much smaller than the second one, we can neglect them. The third term is zero if only one end is charged. Note that eq 34 reduces to 21b when $Q_1 = Q_N = 0$, as it should be. To simplify, we will now write $Q_1 = cQ_N$ (with $Q_N > 0$ and $|c| \leq 1$), to obtain

$$S_\infty^\parallel(\mathbf{q}) \approx 1 - \frac{(z_N^\parallel)^2}{12B^2(c')} + \ldots \approx 1 - \frac{q^2(\xi_N^\parallel)^2}{12B^2(c')} + \ldots \tag{35a}$$

$$B^2(c') = \frac{5}{2(c')^2 - c' + 2} \tag{35b}$$

$$c' = \frac{\langle \cos\theta\rangle_1}{\langle \cos\theta\rangle_N} \tag{35c}$$

It is easy to show that the structure factor of a rod of length L parallel to $\mathbf{q}$ is given by

$$S_\infty^\parallel(\mathbf{q}) = \sum_{mn} \exp\{i\mathbf{q}\cdot[\mathbf{R}_m - \mathbf{R}_n]\} = \frac{2[1 - \cos(qL)]}{q^2L^2} \approx 1 - \frac{q^2L^2}{12} \quad \text{for } qL < 1 \tag{36}$$

Comparing eqs 35 and 36, we can see that the structure factor of our charged chains in the regime $1 > q\xi^\parallel \gg qR_g$ is characteristic of a rod of effective length $\xi_N^\parallel/B(c')$ parallel to $\mathbf{q}$.

As an example, we now look at three special cases, namely, $c = -1$, $c = 0$, and $c = 1$ ($\xi_1^\parallel = \xi_N^\parallel = \xi^\parallel$ for $c = \pm 1$; $\xi_1 = 0$, $\xi_N = \xi^\parallel$ for $c = 0$). From eq 35, we get

$$S_\infty^\parallel(\mathbf{q}) \approx 1 - \frac{q^2(\xi^\parallel)^2}{12} + \ldots \quad \text{for } c = -1 \tag{37a}$$

$$S_\infty^\parallel(\mathbf{q}) \approx 1 - \frac{q^2\left(\left(\frac{2}{5}\right)^{1/2}\xi^\parallel\right)^2}{12} + \ldots \quad \text{for } c = 0 \tag{37b}$$

$$S_\infty^\parallel(\mathbf{q}) \approx 1 - \frac{q^2\left(\left(\frac{3}{5}\right)^{1/2}\xi^\parallel\right)^2}{12} + \ldots \quad \text{for } c = 1 \tag{37c}$$

These results agree nicely with the radii of gyration given by eqs 32. Finally, it is interesting to note that eqs 35 predict that the shortest effective rod length $\xi_N^\parallel/B(c')$ is found for $c' = 1/4$, and not for $c' = 0$, i.e., $c = 0$. This means that more compact conformations are predicted when both ends are charged, with $z_1 = (1/4)z_N$. This surprising result is due to the competition between the length scales $\xi_N^\parallel$ and $\xi_1^\parallel$, which, for $c' = 1/4$, tends to form more compact J-like conformations.

6.5.2. Parallel Structure Factor for $qR_g \ll 1 < q\xi^\parallel$. In this regime of intermediate wavelengths, we begin to investigate the chain conformation, but without going to length scales smaller than the equilibrium radius of gyration R_g. Equations 27–29 then indicate that the $S_\infty^\parallel(\mathbf{q})$ vs q curves should show some oscillatory behavior because of the trigonometric functions sin and cos. For the special cases $c = \pm 1, 0$, we get (note that there is only one $x^\parallel$ and one $z^\parallel$ parameters in these cases)

$$S_\infty^\parallel(\mathbf{q}) \approx \frac{2[1 - \cos(z^\parallel)]}{(z^\parallel)^2} + \ldots \quad \text{for } c = -1 \tag{38a}$$

$$S_\infty^\parallel(\mathbf{q}) \approx -\frac{6\sin(z^\parallel)}{(z^\parallel)^3} + \frac{6}{(z^\parallel)^2} + \ldots \quad \text{for } c = 1 \tag{38b}$$

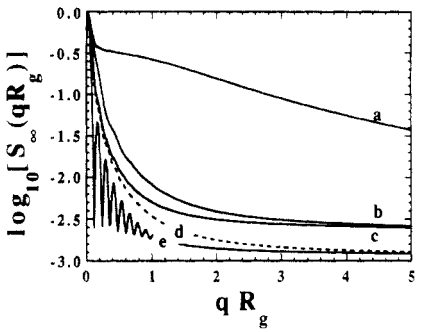

Figure 3. Long-wavelength behavior of the parallel steady-state structure factor: log (S_∞) vs qR_g is plotted for N = 1000 and different end charges. (a) $\Theta_1 = 0$, $\Theta_N = 3$; (b) $\Theta_1 = 1$, $\Theta_N = 3$; (c) $\Theta_1 = -1$, $\Theta_N = 3$; (d) $\Theta_1 = 3$, $\Theta_N = 3$; (e) $\Theta_1 = 3$, $\Theta_N = -3$. Oscillations appear in the parallel direction only when $\Theta_1 \approx -\Theta_N$, i.e., for $c \approx -1$.

$$S_\infty^{\parallel}(\mathbf{q}) \approx \frac{1}{3} + \frac{2e^{-x}\,[5x^{\parallel}\cos(z^{\parallel}) - 2z^{\parallel}\sin(z^{\parallel})]}{(z^{\parallel})^4} + \ldots \quad \text{for } c = 0 \quad (38c)$$

Figure 3 shows $S_\infty^{\parallel}(\mathbf{q})$ vs qR_g curves for different situations. We first see the steep drop in the regime $1 > q\xi^{\parallel} \gg qR_g$ described in section 6.5.1. Following this, the structure factor for the three classes of charged chains is very different. For class a chains with $Q_1 = -Q_N$ or $c = -1$, we see clear oscillations, in agreement with eq 38a; when $Q_1 \neq -Q_N$ however, these oscillations almost disappear. For class b chains, where $1 \geq c > 0$, the oscillations are always very small; since $z^{\parallel} \gg 1$, eq 38b does indeed predict negligible oscillations. For class c chains with $Q_1 = 0$ and $Q_N = Q$, we obtain a very flat line at about log $[S_\infty^{\parallel}(\mathbf{q})] = -0.52$ (or $S_\infty^{\parallel}(\mathbf{q}) = {}^1/_3$), in agreement with eq 38c. These results will be explained below using the theorem we introduced in section 6.2.

When $c < 0$, the end segments point in opposite directions in an electric field. The average chain then assumes an I-shaped conformation (Figure 1). If $Q_1 \neq -Q_N$ however, the electric forces bring in two unequal anisotropic conformation lengths $\xi_1^{\parallel}$ and $\xi_N^{\parallel}$; i.e., the chain is made up of two different parts. Because of the fact that each tube segment has an equal probability of having been oriented by either end segment (section 6.2), the distribution function for the curvilinear lengths of each of these two parts is uniform between 0 and L. For a given conformation, the effective length $\xi_\lambda^{\parallel}$ of the chain along the field direction is thus

$$\xi_\lambda^{\parallel} = \frac{1}{L}\xi_1^{\parallel} + \frac{L-\lambda}{L}\xi_N^{\parallel} \quad (39)$$

where λ is the curvilinear length of the part of the chain oriented by the Q_1 end of the chain. The various molecular conformations simply have different values of λ. The net effective length $\xi_{\text{eff}}^{\parallel}$ is thus the average of the lengths $\xi_\lambda^{\parallel}$ over a uniform distribution function for λ:

$$\xi_{\text{eff}}^{\parallel} = \langle \xi_\lambda^{\parallel} \rangle = \frac{\int_0^L \xi_\lambda^{\parallel}\, d\lambda}{\int_0^L d\lambda} = \frac{\xi_1^{\parallel} + \xi_N^{\parallel}}{2} \quad (40)$$

Similarly, the structure factor is given by the average of the structure factor for all possible values of λ. For $Q_1 = -Q_N$, we have $\xi_{\text{eff}}^{\parallel} = \xi_1^{\parallel} = \xi_N^{\parallel} = \xi^{\parallel}$ and there is no competition between two length scales. The structure factor is characteristic of a rodlike chain (compare eqs 38a and 36) and shows a series of oscillations. For $Q_1 \neq -Q_N$ however, the structure factor is an average over accessible molecular conformations that have two different orientation lengths ($\xi_1^{\parallel}$, $\xi_N^{\parallel}$) and two different oscillation periods $2\pi/\xi_1^{\parallel}$ and $2\pi/\xi_N^{\parallel}$. The result of the superposition of these oscillations is that no net oscillations exist when $\xi_1^{\parallel}$ and $\xi_N^{\parallel}$ are very different.

For class b chains, the electric forces attract both ends of the charged molecule to form, on average, a J-shaped conformation (Figure 1). First, we examine the special case where $Q_1 = Q_N$. Again, there is only one orientation length $\xi_1^{\parallel} = \xi_N^{\parallel} = \xi^{\parallel}$. The lengths λ and $L - \lambda$ of the two arms of the J are uniformly distributed between 0 and L. The structure factor $S_\lambda^{\parallel}(\mathbf{q})$ of one J-shaped chain with arm lengths λ and $L - \lambda$ is easily shown to be given by

$$S_\lambda^{\parallel}(\mathbf{q}) = \frac{1}{N^2}\sum_{mn} e^{i\mathbf{q}\cdot[\mathbf{R}_m - \mathbf{R}_n]} = \frac{2\left\{\cos(q\lambda) - 2\cos\left[\frac{q(L-\lambda)}{2}\right] - 2\cos\left[\frac{q(L+\lambda)}{2}\right] + 3\right\}}{q^2L^2} \quad (41)$$

from which the average structure factor is

$$S = \langle S_\lambda \rangle = -\frac{6\sin(qL)}{q^3L^3} + \frac{6}{q^2L^2} \quad (42)$$

This result is identical to eq 38b with $L \to \xi^{\parallel}$ and leads to very small oscillations (Figure 3). When $Q_1 \neq Q_N$, we have $\xi_1^{\parallel} \neq \xi_N^{\parallel}$, and a calculation similar to the one leading to eq 42 also shows negligible oscillations. Therefore, the lack of coherence of the resulting scattering functions for each value of λ eliminates all oscillations, even when $c = 1$ (i.e., $Q_1 = Q_N$).

For class c, the electric field affects the charged end ($i = N$) and orients a part of the chain, the rest of the chain staying in a random-walk conformation. As before, section 6.2 suggests that the curvilinear length λ of the oriented part is randomly distributed between 0 and L. The effective length of the chain along the field direction is now $\xi_N^{\parallel}/2$. However, since the distance between the segments of the unstretched, random-walk-like conformation near the uncharged end is much smaller than the distance between all the other segments, the major contribution to the static structure factor comes from this part of the chain. The structure factor for a random-walk chain section with a curvilinear length λ gives in the $qR_g < 1$ limit

$$S_\lambda^{\parallel}(\mathbf{q}) \approx \frac{1}{N^2}\sum_{mn}^{\lambda/a} e^{i\mathbf{q}\cdot(\mathbf{R}_m - \mathbf{R}_n)} \approx \frac{1}{N^2}\left(\frac{\lambda}{a}\right)^2 \quad (43)$$

where we used the fact $\mathbf{q}\cdot(\mathbf{R}_m - \mathbf{R}_n) \ll 1$. The average over the values of λ gives

$$S^{\parallel} = \langle S_\lambda^{\parallel} \rangle = {}^1/_3 \quad (44)$$

in agreement with Figure 3 and eq 38c; note that $S_\infty^{\parallel} = {}^1/_3$ for *all* values of Θ_N when $\Theta_1 = 0$.

In conclusion, we find that the theorem described in section 4.2 has a profound influence on the scattering behavior of telehelic ionomers in the wavelength regime where $R_g < 1/q < \xi^{\parallel}$. Because the relative weight of the two ends is uniformly distributed between [0,1], the competition between the two end segments to create new tube sections leads to a polydisperse solution of molecules with a wide range of radii of gyration. The average static structure factor is then featureless, except in the case $c \approx$

-1. When only one end is charged ($c = 0$), scattering comes mostly from the unoriented tube sections and we have a remarkably broad plateau at $S^{\parallel}_{\infty} \approx 1/3$.

6.5.3. Parallel Structure Factor for $1 < q^2R_g^2 < q\xi^{\parallel}$. Using the blob sizes $b_i^{\parallel} = R_g^2/\xi_i^{\parallel}$ introduced before, this regime can also be defined by

$$\frac{1}{q^2R_g^2} < 1 < \frac{1}{qb_i^{\parallel}} \tag{45}$$

The wavelength is thus such that details within a blob cannot be seen ($q^{-1} > b_i^{\parallel}$) while details within a distance R_g will be probed ($q^{-1} < R_g$). This means that the blob structure created by a charged end segment will show up in the scattering function, while the random-walk nature of the tube segments generated by an uncharged end segment will also be present. From eq 27, the structure factor in this limit is given by

$$S^{\parallel}_{\infty}(\mathbf{q}) \approx \frac{x_1^{\parallel}}{(z_1^{\parallel})^2} + \frac{x_N^{\parallel}}{(z_N^{\parallel})^2} + \dots \quad \text{if } c \neq 0 \tag{46a}$$

$$\approx \frac{x_N^{\parallel}}{(z_N^{\parallel})^2} + \frac{1}{x_1^{\parallel}} + \dots \quad \text{if } c = 0 \tag{46b}$$

Using the fact that $x_i^{\parallel}/(z_i^{\parallel})^2 \approx R_g^2/(\xi_i^{\parallel})^2$, we can rewrite these equations as

$$S^{\parallel}_{\infty}(\mathbf{q}) \approx \frac{6(n_1 + n_N)}{N} + \dots \quad \text{if } c \neq 0 \tag{47a}$$

$$\approx \frac{6(n_N)}{N} + \frac{1}{q^2R_g^2} + \dots \quad \text{if } c = 0 \tag{47b}$$

where $n_i = b_i^2/a^2$ is the number of segments contained in a blob of size b_i. Equation 47a thus says that $S^{\parallel}_{\infty}(\mathbf{q})$ should be independent of $\mathbf{q}$ and proportional to the inverse of the number of average blobs forming the chain, $N/(n_1 + n_N)$. Figure 3 clearly shows this regime for $qR_g > 1$. When only one end is charged however, eq 47b indicates that the uncharged end should give rise to a q-dependent term $1/x_1$. This shows as a slowly decreasing function $S^{\parallel}_{\infty}(\mathbf{q})$ on Figure 3 for $\Theta_N = 3$ and $\Theta_1 = 0$. Note that the $1/x_1$ term being the largest term in eq 46b, the scattering function for $c = 0$ (one uncharged end) is much larger than with two charged ends ($c \neq 0$). This comes from the fact that a $c = 0$ chain has a very dense end where the random-walk conformation keeps the segments very close to each other, which increases the scattering substantially.

6.5.4. Parallel Structure Factor for $1 < q\xi^{\parallel} < q^2R_g^2$. In the short-wavelength limit where $q^{-1} < R_g^2/\xi^{\parallel} \equiv b^{\parallel}$, with $\xi^{\parallel} > R_g$, eq 27 reduces to

$$S^{\parallel}_{\infty}(\mathbf{q}) \approx \frac{1}{x_1^{\parallel}} + \frac{1}{x_N^{\parallel}} + \dots \approx \frac{2}{x^{\parallel}} + \dots \tag{48}$$

where $x_1^{\parallel} \approx x_N^{\parallel} \equiv x^{\parallel}$. This result is similar to the one found in section 6.4 for low field intensities ($R_g > \xi^{\parallel}$) or for the transverse static structure factor ($\psi = \pi/2$). Therefore, the long-range deformation due to the electric forces acting on the end segments does not affect the molecular conformations on a short length scale such that $q^{-1} < b^{\parallel}$. This is in agreement with section 6.1.

6.6. Describing the Structure Factor in Terms of the Blob Sizes. Now, let us describe the four regimes described in section 6.5 in terms of the blob sizes b_1 and b_N and the anisotropic lengths $\xi_1^{\parallel}$ and $\xi_N^{\parallel}$. Figure 4 represents "typical" (i.e., average) oriented conformations for the three classes of charged chains showing the breakdown of the chain into two sections with blob sizes b_1 and b_N. For $q > (1/b_1, 1/b_N)$ (section 6.5.4) the electric forces are not strong enough to modify the random-walk nature of the conformation, and the structure factor is that for zero field. In the opposite limit where $q < (1/\xi_1^{\parallel}, 1/\xi_N^{\parallel})$ (section 6.5.1), the blobs are aligned to form a quasi-rod of average length $\xi^{\parallel}/B(c')$. For $1 > R_g > q > 1/\xi^{\parallel}$ (section 6.5.2), the structure factor shows different behaviors for the three types of charged ionomers. When $c < 0$ (class a), we obtain strong oscillations only when $Q_1 \approx -Q_N$ (or $c \approx -1$). When $c > 0$ (class b), we see no oscillation. When $c = 0$ (class c), we obtain a flat line around $S^{\parallel}_{\infty}(\mathbf{q}) \approx 1/3$. Finally, for $(1/b_1, 1/b_N) > q > 1/R_g$ (section 6.5.3), we probe the blob structure of the rod, which leads to a structure factor that is independent of $\mathbf{q}$ and proportional to the reciprocal of the number of average blobs; for class c chains however, the uncharged end dominates and the structure factor still depends on $\mathbf{q}$ because we then probe inside the random-walk end of the conformation. Of course, the high-field limit characterized by the alignment of the blobs makes sense only if $(b_1, b_N) < R_g$ and $(N/n_1, N/n_N) > 1$; these conditions are equivalent to $(\xi_1^{\parallel}, \xi_N^{\parallel}) \gg R_g$ (at least one end segment being charged).

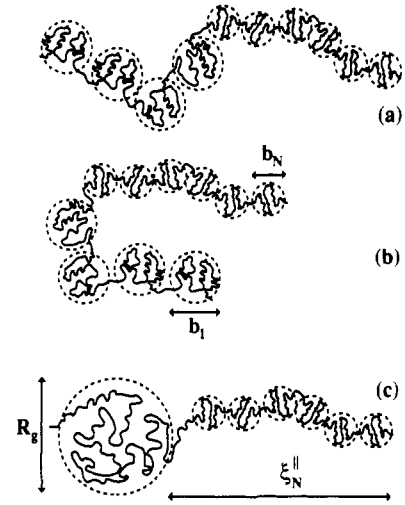

Figure 4. Typical (i.e., average) oriented conformations for the three classes of charged chains with blob sizes b_1 and b_N. (a) $Q_1Q_N < 0$: Two kinds of blobs are aligned to form an I-shaped chain. (b) $Q_1Q_N > 0$: Two kinds of blobs are aligned to form a J-shaped chain. (c) Only one end is charged: One kind of blob (b_N) forms the oriented chain, while the unoriented part has a characteristic size $\approx R_g$.

6.7. Electric Field Dependence of the Structure Factor. We see from Figure 3 that the $S_{\infty}(\mathbf{q})$ vs q curves are very much affected by the electric field at $qR_g \approx 1$ because it is in this wavenumber interval that the derivative of the equilibrium static structure factor $S_{equ}(\mathbf{q})$ is the larger (see curve e on Figure 2).

On Figure 5, we plotted log $[S_{\infty}(qR_g = 1)]$ vs Θ_N for different values of the ratio $c = Q_1/Q_N = \Theta_1/\Theta_N$ and angle ψ. When $c \neq 0$ (class a and b chains), the effect of the field is dramatic at $\psi \neq \pi/2$ since it leads to oriented conformations of size ξ^{ψ}_{eff}. When $c = 0$ (class c) however, most of the scattering comes from those segments near the uncharged end of the molecule. The structure factor is then found to be a flat line (around log $(1/3) \approx -0.523$) for almost all values of the field Θ_N.

In the transverse direction ($\psi = \pi/2$), the average conformation for all classes of charged chains is still

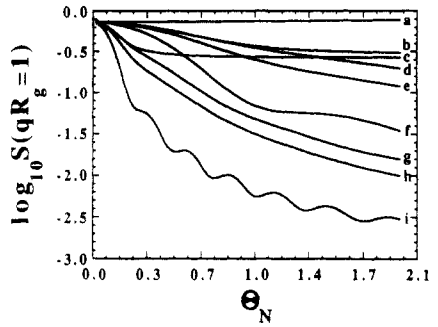

Figure 5. Field dependence of the steady-state structure factor: log $[S_\infty(qR_g=1)]$ vs Θ_N is plotted for $N = 1000$, different angles ψ, and different ratios $c = Q_1/Q_N$ between the end charges. (a) $\psi = \pi/2$, $c = -1$; (b) $\psi = 0$, $c = 0$; (c) $\psi = 5\pi/12$, $c = 0$; (d) $\psi = 5\pi/12$, $c = 1/3$; (e) $\psi = 5\pi/12$, $c = -1/3$; (f) $\psi = 5\pi/12$, $c = -1$; (g) $\psi = 0$, $c = 1/3$; (h) $\psi = 0$, $c = -1/3$; (i) $\psi = 0$, $c = -1$. When $c \neq 0$, the chain dimensions are affected at $\psi \neq \pi/2$. When $c = 0$, the structure factor appears as a flat line.

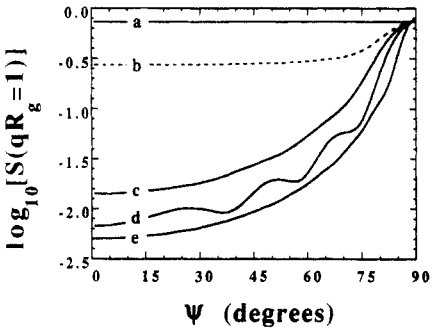

Figure 6. Angular anisotropy of the steady-state static structure factor shown on log $[S_\infty(qR_g=1)]$ vs ψ curves for $N = 1000$ and different end charges. (a) $\Theta_1 = 0$, $\Theta_N = 0$; (b) $\Theta_1 = 0$, $\Theta_N = 1$; (c) $\Theta_1 = 1$, $\Theta_N = 1$; (d) $\Theta_1 = 1$, $\Theta_N = -1$; (e) $\Theta_1 = 1$, $\Theta_N = -3$. For large angles ψ, the structure factor is the same for all cases since large fields are necessary to modify the structure factor near the transverse direction.

random-walk-like, and we need much higher field intensities for the chain dimensions to be affected. Finally, we also notice that some oscillations are present each time the field is such that a peak would appear at $qR_g = 1$ on a $S^{\psi}_{\infty}(\mathbf{q})$ vs qR_g diagram for $c \approx -1$.

6.8. Anisotropy Induced by the Field. The orientation of the chain in the field direction is accompanied by a slight decrease in its transverse dimensions, and the shape of the average chain conformation is an ellipsoid. Figure 6 shows how the static structure factor measures the properties of this ellipsoid. One can see chain dimensions of the order of R_g only for large angle ψ. We also see some oscillations when $c \approx -1$ and a remarkably flat line (around log (1/3) = −0.523) for $c = 0$. Of course, individual conformations (which can be observed by various video-microscopy techniques[7,18]) are expected to be anisotropic even in absence of electric forces, i.e., even if the average conformation is isotropic;[19] the orientation and anisotropy effects discussed in this paper refer to average molecular conformation properties such as those observed by scattering.

7. Discussion

In the biased reptation model,[4,5] originally developed to study DNA gel electrophoresis, the reptating molecule experiences two biases in the presence of an electric field. First, the molecule tends to orient in the field direction because of the electric forces acting on the end segments of the primitive chain. Second, the total force on the molecule leads to a net electrophoretic velocity. These two biases are coupled because the charge is uniformly distributed along the DNA chain; also, the tube orientation increases the electrophoretic velocity. The charges on the end segments have a major impact during reptation since they alone generate the new tubes in which the migration occurs. For example, it was recently shown that reducing the charge on the ends of DNA molecules could greatly increase the separation power of gel electrophoresis.[13] In this article, we studied the opposite situation where the polymer has charges only on or near its ends—hence the name telehelic ionomers.

The electrophoretic migration of these telehelic ionomers in neutral gels, or in dense solutions of neutral polymers, should be very well described by the biased reptation model used here. For example, the absence of charges along the main backbone of the molecule eliminates the growth of hernias and other non-reptation molecular conformations that violate the tube description.[20] Also, the negligible electrophoretic velocity (see next paragraph) will eliminate the "bunching" effect found during DNA gel electrophoresis.[20]

In this article, we assumed that prob $[\eta(t)=+1]$ = prob $[\eta(t)=-1] = {}^1/_2$ in the Langevin equation of motion (1). When this is not the case, an extra term[11] appears in eq 11 and subtle effects may occur, such as those leading to band inversion during DNA gel electrophoresis.[21] This term and the corresponding field-driven electrophoretic velocity can be neglected for long telehelic ionomers when tube renewal is due mostly to the unbiased longitudinal Brownian motion of the chain along its tube axis. For a tube of length Na, the Brownian tube renewal time is simply given by[16,17]

$$\tau_D = N^2 \Delta t \tag{49}$$

where Δt is the average time required by the chain to move over a distance a. The average electric force acting along the tube axis due to a charge Q on one end segment is given approximately by

$$\langle F_1 \rangle \approx QE\langle \cos\theta \rangle \tag{50}$$

which leads to the field-driven tube renewal time

$$\tau_E \cong \frac{Na}{\langle F_1 \rangle / \xi_1} \tag{51}$$

where $\xi_1 = 2k_BT\Delta t/a^2$ is the curvilinear friction coefficient of the chain in its tube. The longitudinal velocity and bias can thus be neglected if

$$\frac{\tau_E}{\tau_D} \approx \frac{3}{N\Theta^2} \gg 1 \tag{52}$$

For experimental values such as $Q = 10$ e, $E = 10$ V/cm, $a = 10$ nm, and $T = 300$K, we obtain a scaled field $\Theta \approx QEa/2k_BT \approx 2 \times 10^{-3}$ and eq 52 requires that $N < 8 \times 10^5$ segments. These values are typical of DNA electrophoresis in polyacrylamide gels. Therefore, we can easily neglect the electrophoretic velocity of telehelic ionomers in most experimentally relevant situations since the Brownian motion dominates the small field-driven longitudinal drift.

When the electrophoretic velocity is negligible, the molecule migrates through normal Brownian motion, and the shape of the molecule is a function of the properties of the tube-creating end segments. This is why the static structure factor $S_\infty(q)$ is found to be a function of the boundary condition parameters $x_{1,N}$ and $z_{1,N}$. The boundary conditions lead to a competition between different length scales. On the one hand, the tendency to optimize the entropy of the molecular conformations is related to

the radius of gyration R_g and to the parameters $x_{1,N}$. On the other hand, charged end segments tend to orient the molecular conformations in the direction of the applied electric field, which leads to the orientation lengths $\xi_{1,N}$ and the parameters $z_{1,N}$. When $\xi^{\parallel} > R_g$, the electric forces substantially deform the molecular conformation. The physics of this effect can be understood quantitatively using two fundamental concepts: (i) charged ends create random-walk blobs of tube sections that align themselves in the field direction; (ii) the number of tube sections created by a given end segment is uniformly distributed between 0 and N, the total length of the molecule. The latter fact has a profound impact of the scattering structure factor of reptating telehelic ionomers. For instance, except for the case where $Q_1 = -Q_N$, we virtually obtain a polydisperse solution of molecules; each molecule is formed of two types of blobs, but the number of such blobs varies randomly from one molecular conformation to another.

Perhaps the most remarkable example of this polydisperse-like behavior is found for molecules with charges only at one end. In this case, our results predict that we should see a rodlike structure for long wavelengths $q^{-1} > \xi^{\parallel}$ but a random-walk structure at intermediate wavelengths $q^{-1} > \xi^{\parallel}$. This leads to a steplike $S^{\parallel}_{\infty}(\mathbf{q})$ vs q curve that is totally different from any curve obtained for molecules having charges on both ends.

In fact, our results suggest a straightforward way to measure the ratio $c = Q_1/Q_N$ between the charges on the two ends of telehelic ionomers. First, for fields small enough that $\Theta_{1,N} < 1$, eqs 34, 13b, and 6b lead to

$$A = \lim_{q\to 0} \frac{1 - S^{\parallel}_{\infty}}{q^2} = \frac{L^2E^2a^2}{2160(k_BT)^2}(2Q_1^2 + 2Q_N^2 - Q_1Q_N) \quad (53)$$

where A is independent of q. Second, from eq 46a we obtain, in the specified regime,

$$B = S^{\parallel}_{\infty}(q) = \frac{6(k_BT)^2}{E^2La}\left(\frac{1}{Q_1^2} + \frac{1}{Q_N^2}\right) \quad (54)$$

which is also independent of q. Finally, from eqs 21b and 33a we get

$$F = R_g^2 = \lim_{\substack{E\to 0 \\ q\to 0}} \frac{3(1 - S(q))}{q^2} \quad (55)$$

From eqs 53–55, we find that the ratio $c = Q_1/Q_N$ is the solution of

$$2c^4 - c^3 + \left(4 - 60\frac{AB}{F}\right)c^2 - c + 2 = 0 \quad (56)$$

This equation is valid only if $\xi_1^{\parallel} > R_g$ and $\xi_N^{\parallel} > R_g$. Since A, B, and F can all be measured experimentally, eq 56 can be used to obtain the ratio $c = Q_1/Q_N$. This could be a way to better characterize a sample of telehelic ionomers.

Adding a few electric charges to the ends of long neutral polymers provides a simple way to orient them in a matrix. Although their electrophoretic velocity is negligible, the reptation mechanism allows the user to orient them using an external electric field. The orientation time is given by eq 49. Note however that unless $Q_1 = -Q_N$, one cannot have a uniform molecular orientation.

In conclusion, we have studied the orientation properties of reptating telehelic ionomers. Such molecules can be synthesized (see ref 10 for some details concerning the chemistry involved). The key to understanding the results of our analytical calculations of the static structure factor is provided by the theorem presented in section 6.2. Unless $Q_1 = -Q_N$, these molecules can be in a wide range of oriented conformations that leads to an average behavior characteristic of a polydisperse solution. When only one end is charged, the static structure factor has a unique steplike shape. Finally, we showed that scattering experiments can be used to measure the charge ratio $c = Q_1/Q_N$. These experiments would be a good test for the reptation model.

Acknowledgment. This work was supported by the Natural Science and Engineering Research Council of Canada. We would also like to thank David Hoagland for a useful discussion.

References and Notes

(1) Chrambach, A.; Rodbard, D. *Science* **1971**, *170*, 440.
(2) Guo, X.-H.; Chen, S.-H. *Phys. Rev. Lett.* **1990**, *64*, 2579.
(3) Smisek, D. L.; Hoagland, K. A. *Macromolecules* **1989**, *22*, 2270.
(4) Lumpkin, O. J.; Déjardin, P.; Zimm, B. H. *Biopolymers* **1985**, *24*, 1573.
(5) Slater, G. W.; Rousseau, J.; Noolandi, J. *Biopolymers* **1987**, *26*, 863.
(6) Smith, S. B.; Aldridge, P. K.; Callis, J. B. *Science* **1989**, *243*, 203.
(7) Schwartz, D. C.; Koval, M. *Nature* **1989**, *338*, 520.
(8) Schwartz, D. C.; Cantor, C. R. *Cell* **1984**, *37*, 67.
(9) Platt, K. J.; Holzwarth, G. *Phys. Rev. A* **1989**, *40*, 7292.
(10) Slater, G. W.; Noolandi, J.; Eisenberg, A. *Macromolecules* **1991**, *24*, 6715.
(11) Slater, G. W.; Noolandi, J. *Macromolecules* **1986**, *19*, 2356.
(12) Lumpkin, O.; Levene, S. D.; Zimm, B. H. *Phys. Rev.* **1989**, *39*, 6557.
(13) Slater, G. W. *J. Phys. II* **1992**, *2*, 1149.
(14) Ulanovsky, L.; Drouin, G.; Gilbert, W. *Nature* **1990**, *190*, 343.
(15) Viovy, J. L.; Défontaines, A. D. In *Pulsed-Field Gel Electrophoresis, Protocols, Methods and Theories*; Burmeister, M., Ulanovsky, L., Eds.; Humana Press: Totowa, NJ, 1992; pp 403–450.
(16) de Gennes, P.-G. *J. Chem. Phys.* **1971**, *55*, 572.
(17) Doi, M.; Edwards, S. F. *J. Chem. Soc., Faraday Trans. 2* **1978**, *74*, 1789.
(18) Smith, S. B.; Aldridge, P. K.; Callis, J. B. *Science* **1989**, *243*, 203.
(19) Rudnick, J.; Gaspari, G. *Science* **1987**, *237*, 384.
(20) Deutsch, J. M.; Madden, T. L. *J. Chem. Phys.* **1989**, *90*, 2476.
(21) Noolandi, J.; Rousseau, J.; Slater, G. W.; Turmel, C.; Lalande, M. *Phys. Rev. Lett.* **1987**, *58*, 2428.